Production Engineering
https://doi.org/10.1007/s11740-023-01241-3

PROCESSES

3D residual stress modelling in turning of AISI 4140 steel

Sangil Han[1] · Frédéric Valiorgue[1] · Mehmet Cici[1] · Herve Pascal[1] · Joël Rech[1]

Received: 31 August 2023 / Accepted: 13 November 2023

Abstract
This study presents a 3D residual stress modelling method in turning of AISI 4140 steel. To carry out this work, we used a recently developed server-based software called MISULAB, which incorporates physically machined surface and 3D thermo-mechanical loadings. Simple longitudinal turning tests and residual stress measurements of the turned surface were conducted, and the effects of the feed rate and tool geometry including a wear zone on the simulation results for the residual stress gradients were considered. Experimental and simulation results on the residual stress gradients induced by longitudinal turning of AISI 4140 steel at two low feed rates (0.05 mm/rev and 0.1 mm/rev) clearly showed the effects of the feed rate on residual stress gradients.

Keywords 3D residual stress modelling · Longitudinal turning · AISI 4140 steel · MISULAB simulation

1 Introduction

It is well known that residual stress generated in a surface by the turning process strongly affects fatigue strength [1]. In particular, axial turning of round bars is widely used in the automobile and aerospace industries, and there is therefore a high demand for accurate predictions of residual stress in the turned surface. Many efforts have been made to simulate and predict the residual stresses arising from the axial turning process. An extensive review of these modelling studies was carried out by Elsheikh et al. [2]. Although a 2D numerical Lagrangian modelling process has been employed, it suffers from some mesh distortion issues [3]. The use of a 2D Arbitrary Lagrangian Eulerian (ALE) formulation can improve these issues [4], but there are still limits on the modelling of the residual stresses in the actual 3D axial turning process in industry. To meet these requirements when simulating the 3D axial turning process, 3D Lagrangian modelling software such as DEFORM 3D has been employed. 3D modelling has the advantage of enabling the user to model and import complicated tool insert geometries, such as chamfer and to predict the residual stress in the turned surface fairly accurately [5]. However, 3D Lagrangian modelling software always involves chip formation, which requires long computation time, and these models can only simulate a single cut of the tool on the surface. Valiorgue et al. [6] showed that at least five revolutions were needed to reach a steady state for the residual stress during the axial turning process. It is therefore necessary to take into consideration these multiple revolutions when modelling the residual stress during turning. However, current chip separation approaches to the 3D Lagrangian modelling of turning have difficulties in integrating this multi-revolution process due to the long computation times involved. To overcome these difficulties, researchers [6] have applied equivalent thermo-mechanical loadings to the machined surface over five paths without chip formation, and have obtained good agreement with experimental values for the residual stress. Mondelin et al. [7] also reported good agreement for residual stress predictions in the turning of 15-5PH using this type of hybrid model.

The machined surface forms a cylindrical groove, the shape of which depends on the tool tip radius, R_ϵ, and machining parameters such as the feed, f, and depth of the cut, a_p as shown in Fig. 1.

Motivated by this principle, Dumas et al. [8] modelled the physical shape of the turned surface and applied 3D equivalent thermo-mechanical loadings. They reported improved values for the residual stress predictions, especially in the cutting direction. Recently, this new hybrid model with 3D

✉ Sangil Han
sangil.han@enise.fr

[1] Ecole Centrale de Lyon - ENISE, LTDS, UMR CNRS 5513, 58 Rue Jean Parot, Saint-Étienne 42023, France

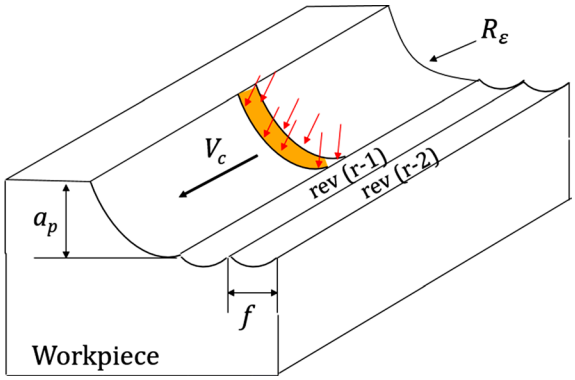

Fig. 1 Modelling of the machined surface

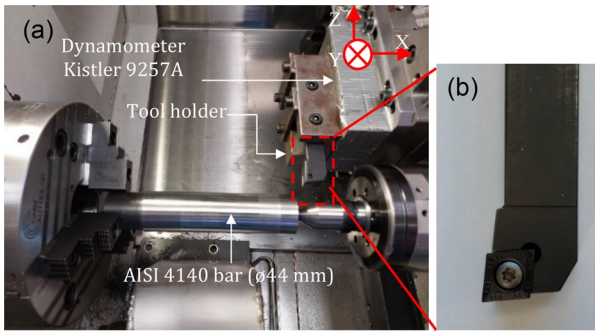

Fig. 2 (**a**) Experimental setup used for turning of the AISI 4140 steel; (**b**) zoomed view showing the insert and tool holder

Table 1 Tool geometry

Parameter	Value
Edge length (mm)	12
Edge sharpness radius (mm)	0.06
Insert angle (°)	80
Insert tip radius (mm)	0.4

equivalent thermo-mechanical loadings was integrated into a server-based software called MISULAB. Extensive efforts have been made to model the residual stress in materials such as AISI 52,100, AISI 316 L, IN 718, Ti-6Al-4 V [9]. While 2D and 3D FEM models of the turning of AISI 4140 steel have been extensively studied, most of these studies have focused on 2D orthogonal machining in order to study the nanocrystal layer [10, 11], white layer [12], and residual stress [13]. A few 3D FEM models based on chip formation have been studied to predict surface roughness [14], but to date, only one 3D model of the residual stress in turning of AISI 4140 steel [15] has been attempted. There is therefore a need to perform simulations of the residual stress gradient in the turning of AISI 4140 steel with the new hybrid 3D model developed by Dumas et al. [8].

In addition, the finishing conditions require low values for the feed rate (less than 0.1 mm/rev) and depth of cut (less than 0.2 mm) in turning, and data on residual stress gradients in surfaces turned at these low values are still lacking. There is therefore a need to measure and simulate residual stress gradients in surfaces turned at small values for the feed and depth of cut.

To address these two major requirements, this study presents experimental measurements of residual stress gradients produced from the turning of AISI 4140 steel at low values for the feed ($f = 0.05$ and 0.1 mm/rev) and depth of cut ($a_p =$ 0.2 mm). We also carry out a 3D simulation with equivalent thermo-mechanical loadings. The effects of the actual tool geometry, such as a small wear zone in a new tool insert, on the residual stress calculations are also investigated. The following sections describe these procedures in detail.

2 Materials and methods

2.1 Material and experimental setup

AISI 4140 steel (also known as 42CrMo4) is considered here as a material due to its widespread use in industry. The experimental setup used to turn the AISI 4140 steel is shown in Fig. 2. An AISI 4140 bar with a diameter of 44 mm and a surface hardness of 35 HRC was positioned in a CNC turning machine (CMZ TC25Y) as shown in Fig. 2(a), and a dynamometer (Kistler 9257 A) was used to measure the experimental cutting forces during turning. A tool insert (CCMT120404-RP4 WPP20S) and a tool holder (SCLCR2020K12) were used as shown in Fig. 2(b). The parameters defining the tool geometry are summarised in Table 1. Turning was performed at a cutting speed of $V_c = 200$ m/min, at low values for the feed rate ($f = 0.05$ and 0.1 mm/rev) and depth of cut $a_p =$ 0.2 mm. A cutting length of $L = 20$ mm was used. Before the cutting tests were carried out, a rough cut was conducted with a depth of cut $a_p = 0.2$ mm, cutting speed $V_c = 100$ m/min, and feed rate $f = 0.05$ mm/rev, with a new tool. All the residual stresses in the workpiece were removed by rough cutting in this way before the machining experiments. No lubrication was used in any of the cutting processes in this study. All three components of the experimental force (i.e. the feed force, $F_{X(EXP)}$, cutting force, $F_{Y(EXP)}$, and penetration force, $F_{Z(EXP)}$) were measured during turning.

The clearance faces of a new insert before and after one cutting test are compared in Fig. 3. A very small wear zone of 30 µm can be observed in Fig. 3(b). This wear zone was considered when modelling the tool geometry in the ABAQUS simulation, as described in the next section. The machined surfaces were analysed via X-ray diffraction (XRD) to obtain the residual stress gradients, using an X-ray diffractometer (Proto). The parameters for the XRD measurements are given in Table 2.

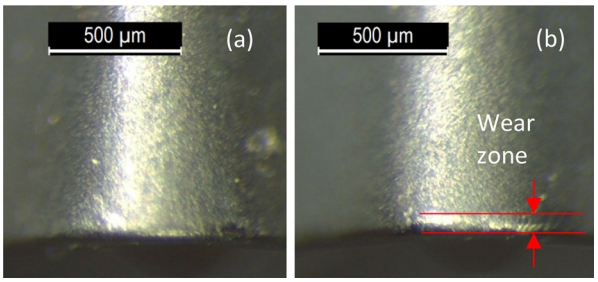

Fig. 3 Optical images of the clearance faces of the tools: (**a**) an unused new tool, (**b**) a used tool with a wear zone (30 µm)

Table 2 XRD parameters for the analysis of residual stress gradients in a turned surface of AISI 4140

Parameter	Value
Diffraction condition	Cr Kα radiation with 18 kV, 4 mA
Wavelength	λ=2.291 nm
-S1 (v/E)	1.237×10^{-3} GPa^{-1}
S2/2 (1+v)/E	5.709×10^{-3} GPa^{-1}
Plan { h k l }	{ 2 1 1 }
Bragg angle	$2\theta = 156.08°$
Beam size	ø2 mm
Polishing strategy	Electropolishing process

Table 3 Thermophysical properties of AISI 4140 steel [16]

Parameter	Temperature (°C)	Value
Thermal conductivity (W/m/°C)	20	43.6
	200	41.7
	400	38.0
	600	32.8
Specific heat (J/kg/°C)	20	437
	200	477
	400	523
	600	568
Density (kg / m^3)	20	7,844
	1,000	7,434
Young's modulus (MPa)	20	212,000
	1,200	137,530
Thermal expansion coefficient (/°C)	0	0
	20	0
	23	0.00001120
	700	0.00001460
Poisson's coefficient ( )	-	0.289

3 Simulations

After the experiments had been carried out, a 3D simulation was conducted with MISULAB commercial software. The details of the simulation procedure are described in the article published by Dumas et al. [8]. The MISULAB simulation involved six steps, as shown in Fig. 4. The thermophysical properties [16] of AISI 4140 steel used in the simulation are given in Table 3.

As a constitutive law for the workpiece material, the Johnson-Cook (JC) model was employed, and the relevant coefficients are given in Table 4. A carbide tool was used in this study. The properties of the tool material and the coefficients of friction between the workpiece and tool surfaces are given in the paper by Dumas et al. [8].

In Step 1 of the MISULAB simulation, as shown in Fig. 4(a), we considered a series of 2D orthogonal cut sections (CSs) with a local uncut chip thickness of $h=0.01$, 0.03, 0.05, 0.07, and 0.09 mm.

In Step 2, as shown in Fig. 4(b), an ABAQUS simulation was conducted in order to obtain the 2D equivalent loading. In their study, Dumas et al. [8] carried out a 2D ALE orthogonal cutting simulation. Recently, Aridhi et al. [17] showed that a 2D CEL orthogonal cutting simulation had a reduced preparation time and advantages in massive simulation; in this work, a 2D CEL orthogonal cutting simulation was therefore employed. The actual tool geometry after one cut was considered in the ABAQUS calculation. A wear zone of length 30 µm was added immediately after the edge radius of $R_\beta = 60$ µm, as shown in Fig. 5(d).

A friction model [17] for the turning of AISI4140 steel with an Al_2O_2/TiCN coated carbide tool was employed as expressed in Eq. (1):

$$\mu = 2.12\, V_s^{-0.45} \tag{1}$$

The friction coefficient, µ, is dependent on the sliding velocity, V_s. This friction model was applied to the contact between the tool and the workpiece.

Thermo-mechanical loadings were calculated for five uncut chip thicknesses ($h=0.01$, 0.03, 0.05, 0.07, and 0.09 mm), based on the heat flux density, *HFL* (W/mm^2), tangential pressure, *S12* (MPa), and normal pressure *S22* (MPa). Examples of the extractions of thermo-mechanical loadings (*HFL*, *S22*, *S12*) for $h=0.05$ mm and their approximations are shown in Fig. 6. In this coordinate system, the origin (Y=0, Z=0) is defined at the centre of the edge sharpness radius (shown by the red dotted circle). Extraction of loadings were made at the machined surface indicated by the extraction line (white solid line). The shape of the extracted HFL is approximated as a polygon composed of four points in Fig. 6(a). The shapes of the extracted S22 and S12 are approximated to triangles in Fig. 6(b) and (c).

Table 4 Johnson-Cook model parameters for AISI 4140 steel [16]

A (MPa)	B (MPa)	n	C	$\dot{\epsilon}_0$	m	T_m (°C)	T_o (°C)
598	768	0.209	0.0137	1	0.807	1520	25

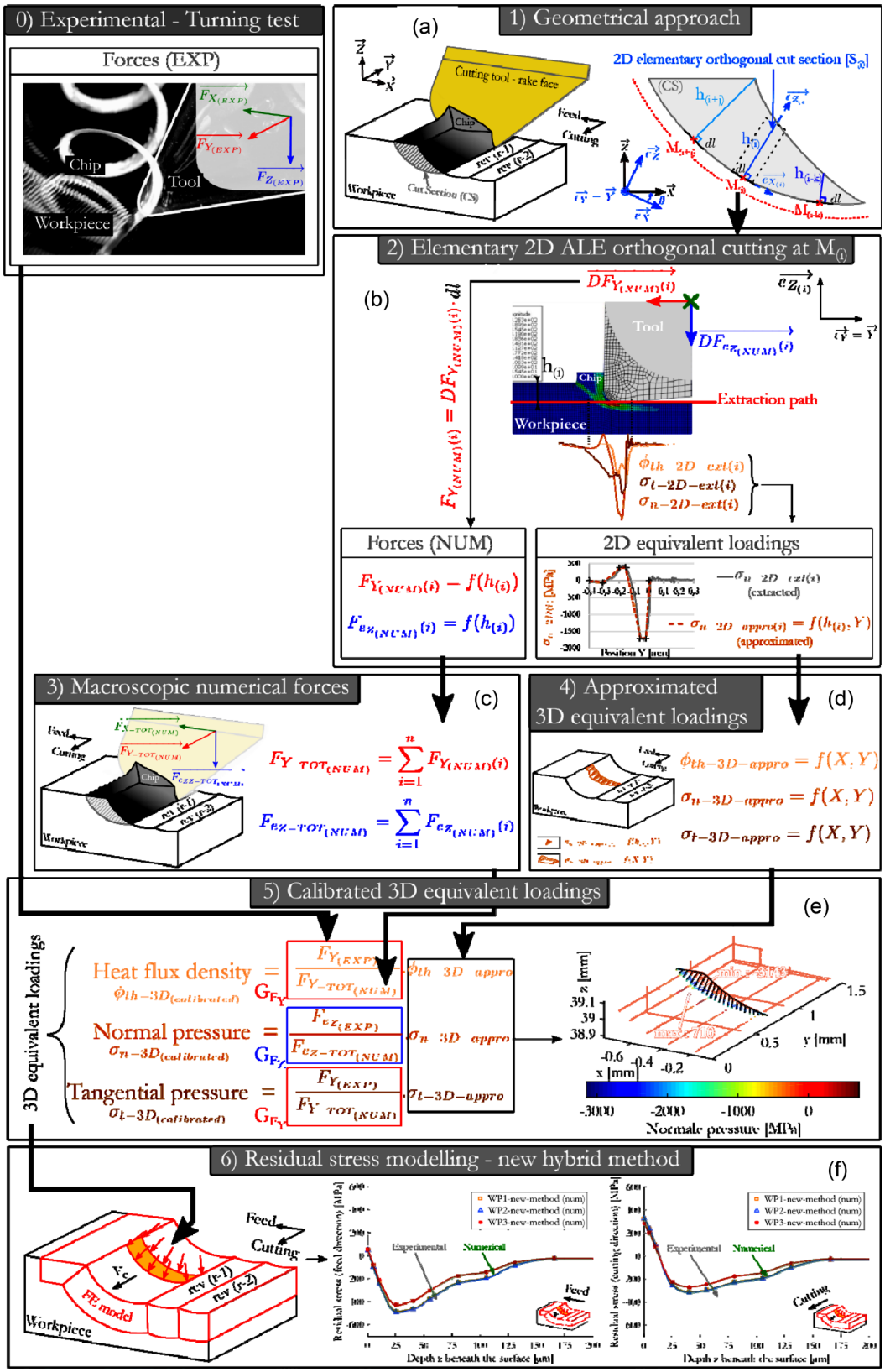

Fig. 4 Schematic diagram of the MISULAB simulation (from Dumas et al. [8] Elsevier © with written permission)

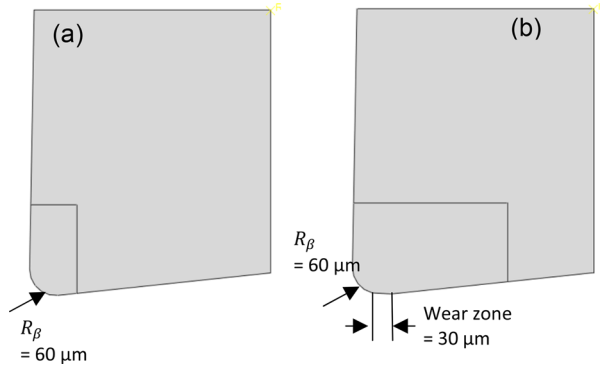

Fig. 5 Tool geometry: (**a**) a new, unused tool; (**b**) a tool with a wear zone of 30 µm

The local cutting and penetration forces, F_Y and F_Z, for the two types of tool (unused and with a wear zone) are compared in Fig. 7. The local values of F_Y and F_Z for the tool with a wear zone are higher than for the unused tool, as there is additional contact between the workpiece and the small wear zone.

In Step 3, as shown in Fig. 5(c), the macroscopic numerical cutting force, $F_{Y-TOT(NUM)}$, and penetration force, $F_{Z-TOT(NUM)}$, were calculated in ABAQUS Explicit. These numerically calculated macroscopic forces may increase with the local cutting and penetration forces, F_Y and F_Z. The experimental and numerically calculated values for the macroscopic forces for the two feeds (f = 0.05 and 0.1 mm/rev) depending on the tool geometry are shown in Tables 5 and 6, respectively.

In Step 4, as shown in Fig. 5(d), approximated 3D equivalent loadings were applied to the round machined surfaces. A calibration step was required for these thermo-mechanical loadings to compensate for the inaccurate estimation from the 2D CEL numerical calculation with ABAQUS Explicit.

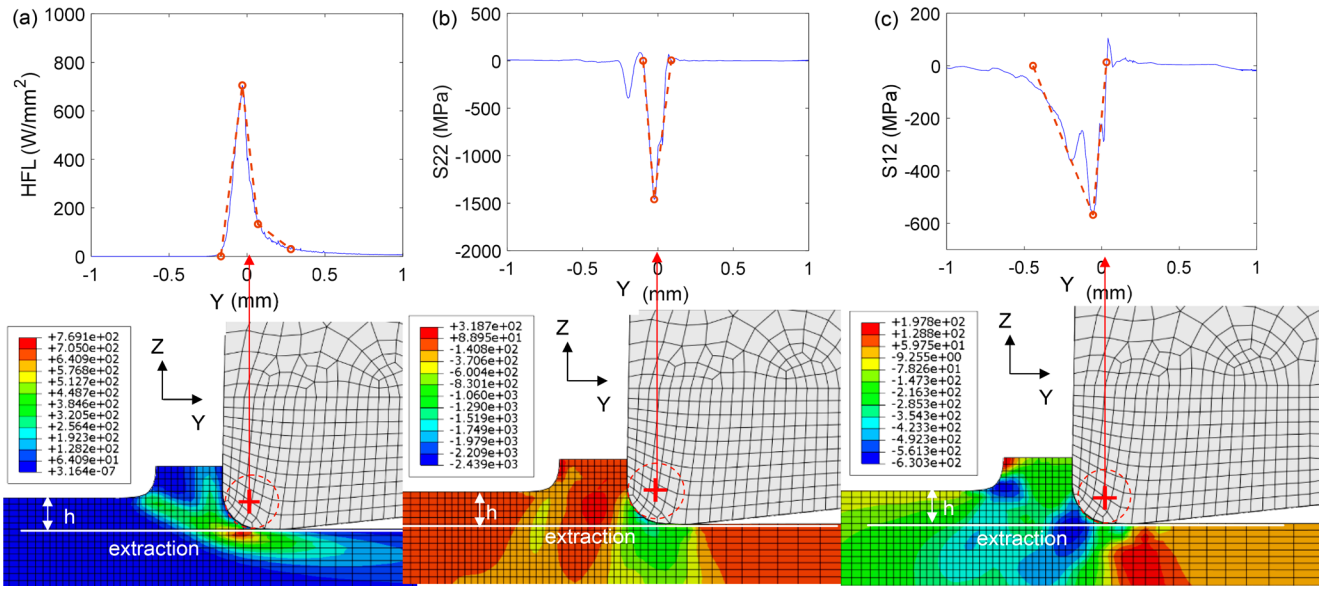

Fig. 6 Extractions of thermo-mechanical loadings with h = 0.05 mm and a tool with a wear zone of 30 µm, and approximations using (**a**) *HFL*, (**b**) *S22*, (**c**) *S12*

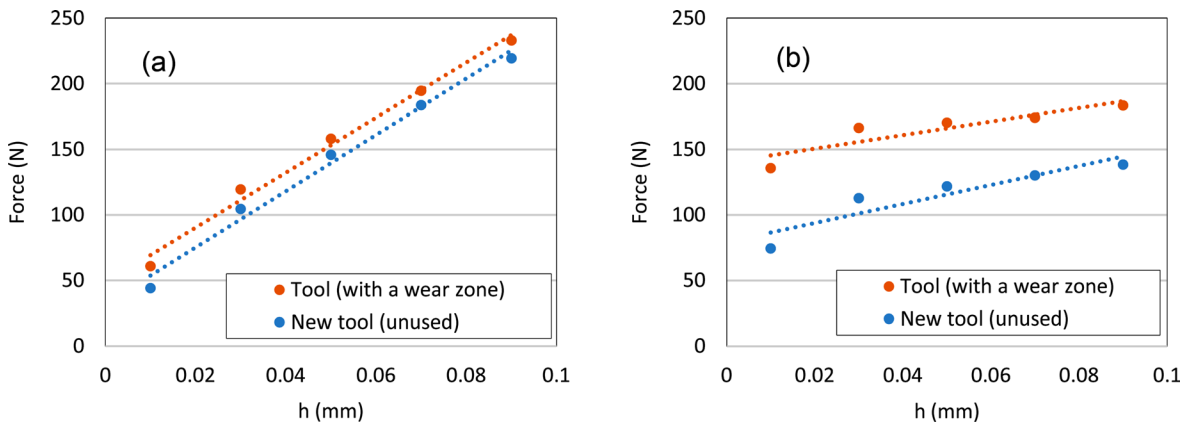

Fig. 7 Local forces for two tools (unused and with a wear zone): (**A**) cutting force, F_Y, and (**b**) penetration force, F_Z

In Step 5, shown in Fig. 5(e), this compensation process was carried out. Based on the experimental values for the cutting force, $F_{Y(EXP)}$, penetration force, $F_{Z(EXP)}$, measured in Sect. 2, the ratios G_{FY} and G_{FZ}, were defined as in given in Eq. (2):

$$G_{FY} = \frac{F_{Y(EXP)}}{F_{Y-TOT(NUM),}} G_{FZ} = \frac{F_{Z(EXP)}}{F_{Z-TOT(NUM),}} \quad (2)$$

Values of G_{FY} and G_{FZ} for the two feeds (f=0.05 and 0.1 mm/rev) are also given in Tables 5 and 6.

The 3D equivalent calibrated loadings for the two feeds (f=0.05 and 0.1 mm/rev), i.e. *HFL*, *S22*, and *S12*, are shown in Fig. 8 (b–d) and Fig. 9(b–d).

The cut sections are also indicated. A comparison of Figs. 8 and 9 shows that the higher feed (f=0.1 mm/rev) had a greater cut section than the smaller feed (f=0.05 mm/rev).

The final step (Step 6), as shown in Fig. 5(e), was performed using the SYSWELD (implicit) solver. It can be seen from Fig. 8(a) and Fig. 9(a) that two different 3D finite elements were generated, representing a physical surface machined with two values for the feed (f=0.05 and 0.1 mm/rev). The elements and mesh sizes are given in Table 6. The 3D equivalent loadings were applied to each 3D finite element. Eight revolutions were simulated in SYSWELD.

3.1 Effects of the small wear zone on macroscopic numerical forces and thermomechanical loadings

After integrating the wear zone of 30 µm in the tool geometry into the ABAQUS calculation, the effects of the wear zone on the macroscopic numerical forces and thermomechanical loadings were analysed.

For the smaller feed rate of f=0.05 mm/rev, the results (as given in Table 5) were as follows:

- The numerical cutting force, $F_{TOT\text{-}Y}$, increased from 37 to 43 N, and the numerical penetration force, $F_{TOT\text{-}Z}$, increased from 35 to 56 N.
- As a result, G_{FY} decreased from 1.26 to 1.08, and G_{FZ} decreased from 1.57 to 1.00.
- Consequently, the calibrated maximum values for *HFL*, *S22*, *S12* in the SYSWELD calculation decreased.

For the higher feed rate of f=0.1 mm/rev (as given in Table 6), similar trends were seen in the macroscopic numerical forces, $F_{Y-TOT(NUM)}$ and $F_{Z-TOT(NUM)}$, the values of G_{FY} and G_{FZ}, and the calibrated maximum values for *HFL*, *S22* and *S12*. By considering this actual tool geometry integration and adjusting the G_{FY} and G_{FZ} values, the calculated residual stress gradients are analysed in Sect. 4.2.

3.2 Effects of feed rate on thermomechanical loadings

In the 3D equivalent calibrated loadings, the cut sections are indicated. A comparison of Figs. 8 and 9 shows that the higher feed (f=0.1 mm/rev) had greater cut section than the smaller feed (f=0.05 mm/rev). However, the maximum values of *HFL*, *S22*, *S12* for these two feeds are very close.

For the higher feed rate of f=0.1 mm/rev, larger surface regions representing previous revolutions can be seen, indicated as "rev(r − 1)", Possible reasons for this geometrical difference in the 3D FEM between the two feeds (0.05 mm/rev vs. 0.1 mm/rev) on residual stress gradients will be discussed in Sect. 4.2.

Table 5 Experimental and numerical forces for two tool geometries: values for G_{FY} and G_{FZ} and calibrated maximum thermomechanical values for a feed of f=0.05 mm/rev

Tool geometry	f=0.05 mm/rev	$F_{(EXP)}$ (N)	$F_{(NUM)}$ (N)	G_{FY}	G_{FZ}	Calibrated maximum values (by multiplying G_{FY})		
						HFL (MPa)	*S22* (MPa)	*S12* (MPa)
New tool (unused)	F_{TOT-Y} (cutting) (N)	46	37	1.26		829		−756
Used tool (with a wear zone)	F_{TOT-Y} (cutting) (N)	46	43	1.08		770		−569
Tool geometry	***f*=0.05 mm/rev**	***F*$_{(EXP)}$ (N)**	***F*$_{(NUM)}$ (N)**	***G*$_{FY}$**	***G*$_{FZ}$**	**Calibrated maximum values (by multiplying*G*$_{FZ}$)**		
						***HFL* (MPa)**	***S22* (MPa)**	***S12* (MPa)**
New tool (unused)	F_{TOT-Z} (penetration) (N)	56	35		1.57		−2,454	
Used tool (with a wear zone)	F_{TOT-Z} (penetration) (N)	56	56		1.00		−1,626	

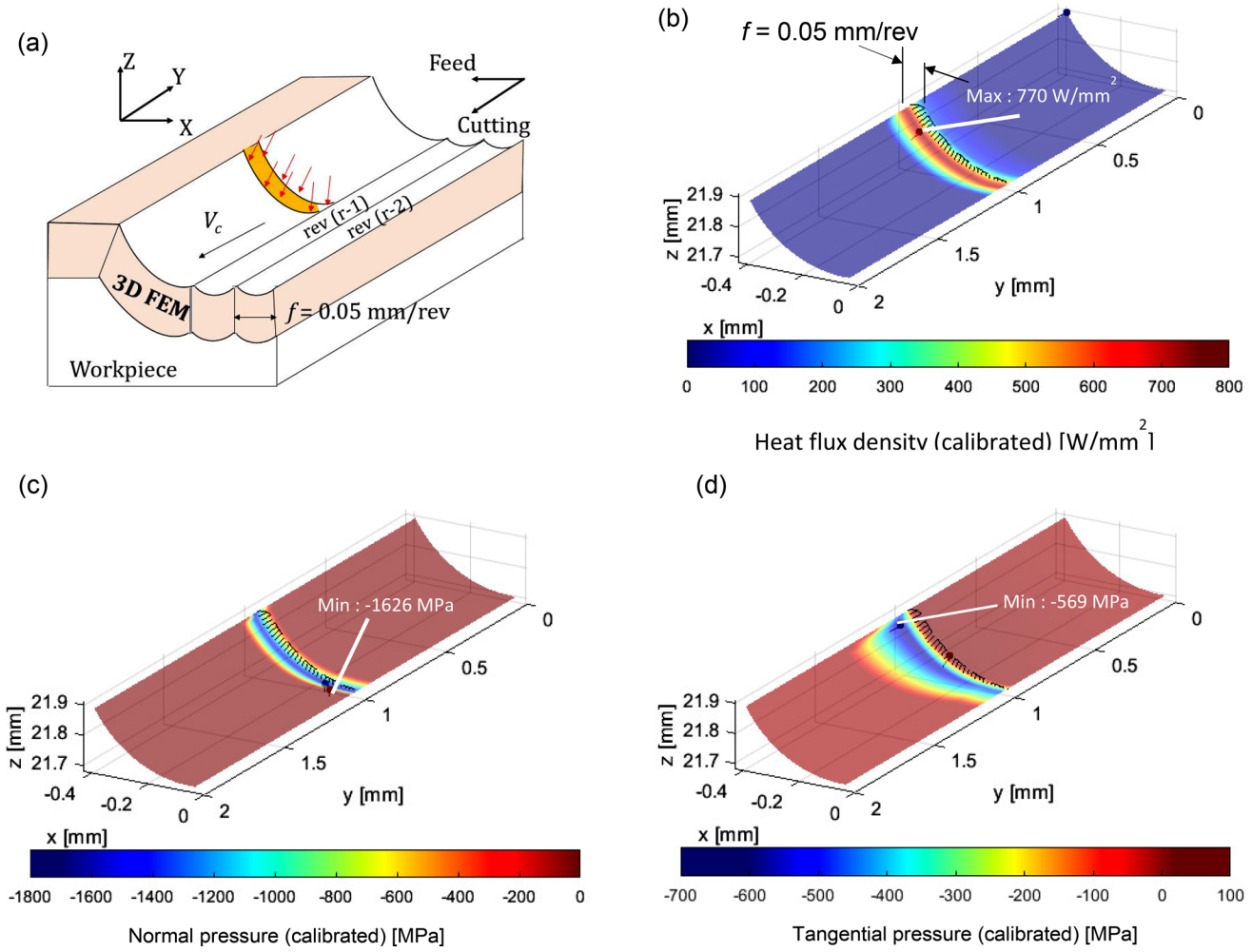

Fig. 8 (**a**) 3D finite element model, (**b**) *HFL*, (**cc**) *S22*, (**d**) *S12* for turning with a feed of f = 0.05 mm/rev and a tool with a wear zone

Table 6 Experimental and numerical forces for two tool geometries: values for G_{FY} and G_{FZ} and calibrated maximum thermomechanical values for a feed of $f = 0.05$ mm/rev

Tool geometry	$f = 0.05$ mm/rev	$F_{(EXP)}$ (N)	$F_{(NUM)}$ (N)	G_{FY}	G_{FZ}	Calibrated maximum values (by multiplying G_{FY})		
						HFL (MPa)	*S22* (MPa)	*S12* (MPa)
New tool (unused)	F_{TOT-Y} (cutting) (N)	69	60	1.13		736		−678
Used tool (with a wear zone)	F_{TOT-Y} (cutting) (N)	69	65	1.05		741		−571
Tool geometry	***f* = 0.01 mm/rev**	$\boldsymbol{F_{(EXP)}}$ **(N)**	$\boldsymbol{F_{(NUM)}}$ **(N)**	$\boldsymbol{G_{FY}}$	$\boldsymbol{G_{FZ}}$	**Calibrated maximum values (by multiplyingG_{FZ})**		
						HFL **(MPa)**	***S22*** **(MPa)**	***S12*** **(MPa)**
New tool (unused)	F_{TOT-Z} (penetration) (N)	63	43		1.46		−2,231	
Used tool (with a wear zone)	F_{TOT-Z} (penetration) (N)	63	62		0.01		−1,624	

Table 7 Elements and mesh size for AISI 4140 turning simulation using SYSWELD (code given in [8])

Symbol	Parameter	Value
La	AFTER element length (mm)	0.03
L_s	CURRENT element length (mm)	0.03
L_b	BEFORE element length (mm)	0.09
T_s	Element thickness (mm)	0.01
T	Mesh thickness (mm)	2
D_s	Finite element depth (mm)	0.003
$D1$	Upper depth (mm)	0.25
D	Total depth (mm)	1
B_{d1}	Upper bias	1.4
B_{d2}	Lower bias	1.6

4 Results and discussion

4.1 Experimental results

The measured residual stress profiles in both the feed and cutting directions are presented in Fig. 10. A traditional hook shape is observed for all of the measured residual stresses. The effects of the feed on residual stress profiles can be clearly seen, as the overall profile for the higher feed is broader; in other words, the affected depth for the higher feed of $f = 0.1$ mm/rev is greater than for $f = 0.05$ mm/rev. When the feed is increased from $f = 0.05$ to 0.1 mm/rev, higher tensile surface residual stresses are observed in both the feed and cutting directions in Fig. 10.

This observation is consistent with those of previous studies. Capello [18] reported that the surface residual stresses became more tensile as the feed increased from 0.05 to 0.25 mm/rev in the turning of Fe370 steel. Sharman et al. [19] observed higher tensile residual stress as the feed was increased from 0.15 to 0.25 mm/rev for the turning of Inconel 718.

Regarding the feed rate in the cutting condition, we can use as a benchmark the machining conditions summarised in a review paper [20] on the turning of AISI 4340 steel (40NiCrMo7). A summary of the machining conditions is given, with the normal feed ranging from 0.1 to 0.3 mm/rev. Among 20 references, only two papers adopted a feed of

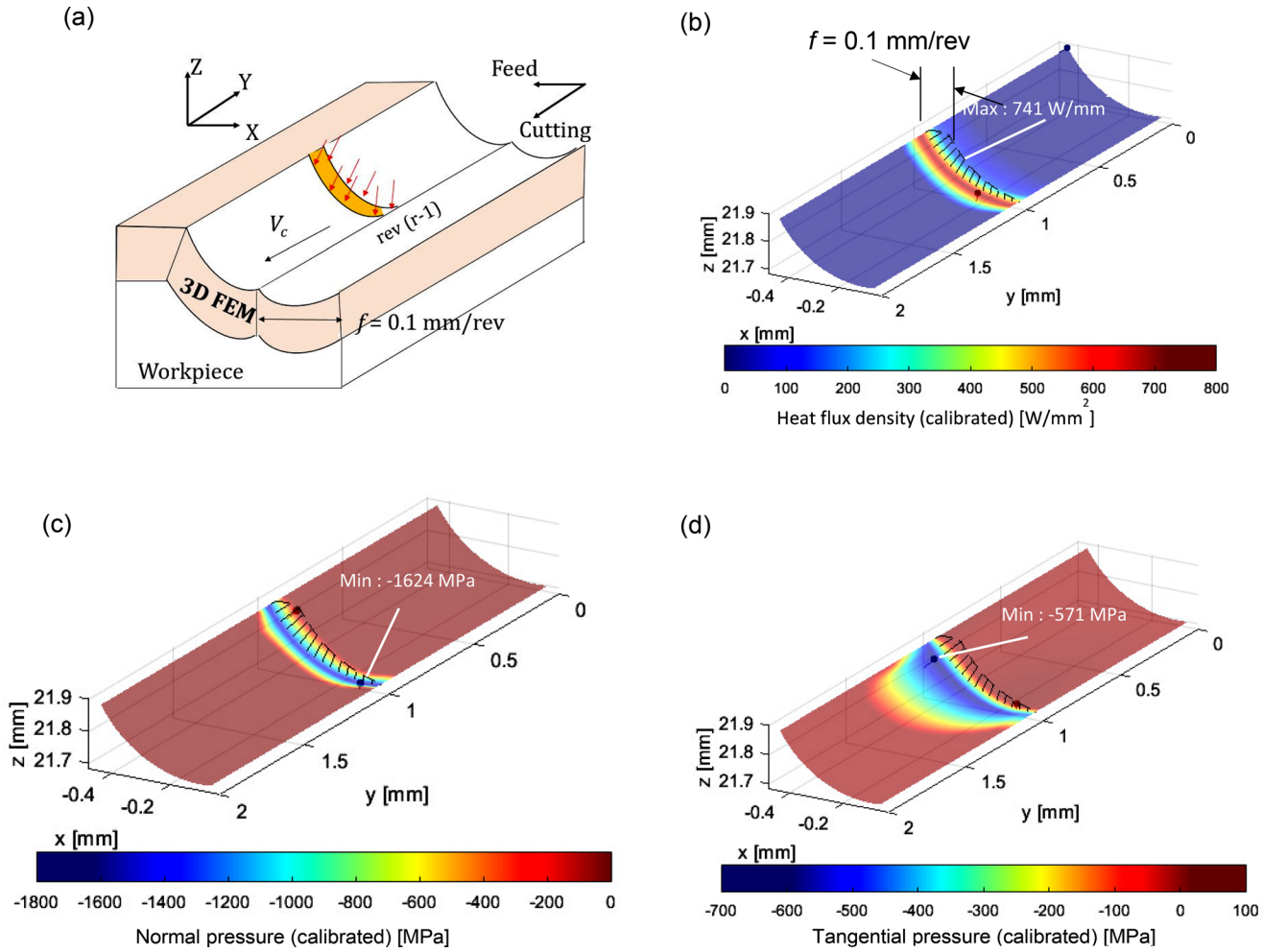

Fig. 9 (**a**) 3D finite element model, (**b**) *HFL*, (**c**) *S22*, (**d**) *S12* for turning with a feed of $f = 0.1$ mm/rev and a tool with a wear zone

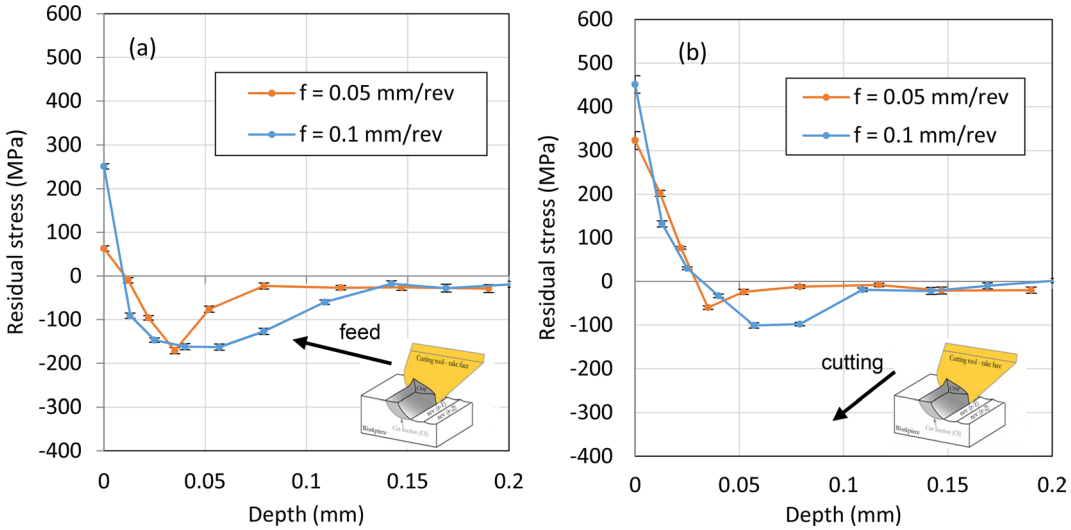

Fig. 10 Experimental residual stress profiles in: (**a**) the feed direction, and (**b**) the cutting direction

0.05 mm/rev to study the cutting force and surface roughness, and these two studies did not include the residual stress.

This study was carried out as a part of the CIRP surface conditioning project [21]. In this project, the reference condition was fixed, with a feed $f = 0.05$ mm/rev, a cutting speed $V_c = 200$ m/min, and a depth of cut $a_p = 0.2$ mm. Both our experimental data and the calculated values for the residual stress under this reference condition are novel, and contribute to the current knowledge of the turning of AISI 4140 steel. In the next section, we present 3D residual stress profile predictions for these cutting conditions, and describe the validation process.

4.2 3D hybrid residual stress model: prediction and validation

4.2.1 Sensitivity study of the input parameters for 3D hybrid residual stress modelling

As stated earlier, this study was done as a part of the CIRP surface conditioning project [21]. The same AISI 4140 (42CrMo4) material and the same tool insert (CCMT120404-RP4 WPP20S) were distributed to several sites to conduct turning, and the residual stress was measured at each site (internal round robin test).

At our site, this grade of AISI 4140 (42CrMo4) was new, because we used AISI 4140 steel (42CD4 grade, as specified by French standards). Several sensitivity studies were therefore conducted to explore the response of the residual stress gradient to the following input parameters: (i) the thermal physical properties (temperature dependent properties vs. constant properties), as given in Table 3; (ii) the coefficients (A, B, C, m, and n) of the constitutive Johnson-Cook model given in Table 4, (iii) the element and the mesh size for the workpiece in SYSWELD simulation (Table 7), and (iv) the tool geometry, which was used in the ABAQUS simulation to consider the actual tool wear.

Of these parameters, we found that the residual stress gradient was very sensitive to a small wear zone in the tool in this 3D hybrid model. When the other parameters were varied, the residual stresses did not change significantly, with a variation within 50 MPa. We therefore present only the results for the change in the wear zone in the following section.

4.2.2 Comparison between experimentally measured and calculated residual stress gradients

4.2.2.1 Effect of actual tool geometry on calculation of residual stress gradients In this section, measured (exp.) and calculated (cal.) results for the residual stresses are compared. Experimental and numerical residual stress gradients for the two types of tool (unused and with a wear zone) are shown in Fig. 11. All of the residual stress gradients for the unused new tool in Fig. 8(a–d) were more compressive than for the tool with a wear zone. As discussed in Sect. 3.1, the numerically calculated macroscopic forces, F_{TOT-Y} and F_{TOT-Z}, increased for the tool with a wear zone, and as a result, the corresponding G_{FY} and G_{FZ} values and thermomechanical loadings decreased.

The values of G_{FZ} decreased from 1.57 to 1.00 for $f = 0.05$ mm/rev (Table 5) and from 1.41 to 1.01 for $f = 0.1$ mm/rev (Table 6). Consequently, significant decrease in normal pressure, *S22* values can cause residual stress gradients with a wear zone to be less compressive. Thus, the residual stress gradients for the tool with a wear zone are close to the experimentally measured values.

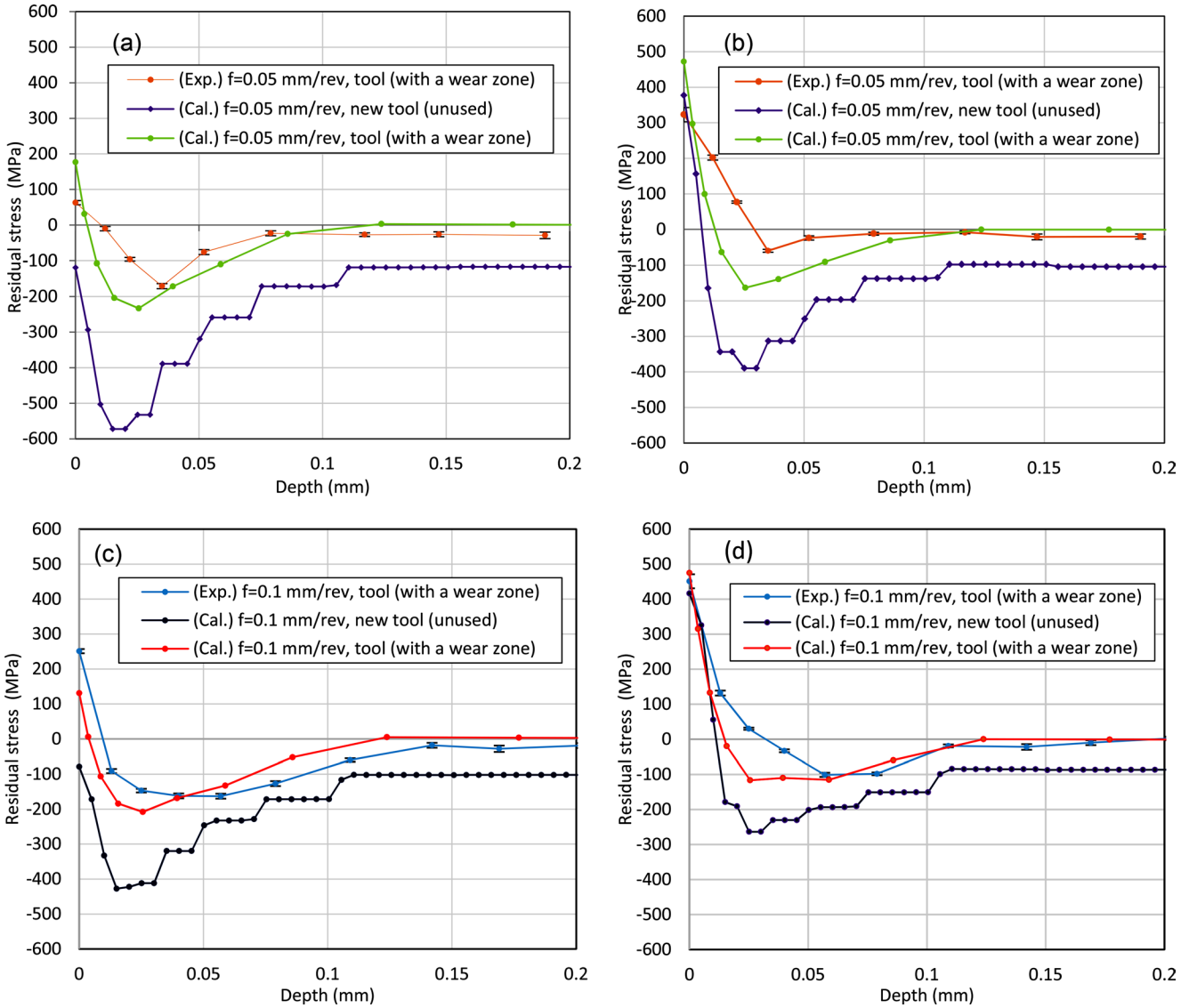

Fig. 11 Experimental and numerical residual stress gradients for two types of tool (unused and with a wear zone) in the turning of AISI 4140 steel: (**a, b**) $f = 0.05$ mm/rev, in the feed and cutting directions, and (**c, d**) $f = 0.1$ mm/rev in the feed and cutting directions

As shown in Fig. 11, good agreement between the measured and calculated residual stress gradients was seen thanks to our hybrid model approach. The overall shapes of the calculated residual stress profiles for the two machining conditions were very similar to the measured results for the residual stress.

4.2.2.2 Effect of feed rate on calculation of residual stress gradients The residual stress in the cutting direction for a higher feed ($f = 0.1$ mm/rev), shown in Fig. 11(b), has broader profiles than for the lower feed ($f = 0.05$ mm/rev), shown in Fig. 11(d). This may be due to the larger regions (0.05 mm/rev vs. 0.1 mm/rev, shown in Fig. 8(a) and Fig. 9(a)) representing previous revolutions, which are indicated as "rev(r − 1)". Although the maximum numerical thermomechanical loading values for the two feeds are not significantly different, as shown in Fig. 8(b–d) and Fig. 9(b–d), thermomechanical history transfer [8] can occur in the larger regions of 0.1 mm at the higher feed than that of 0.05 mm at lower feed. Thus, the larger regions at higher feed of 0.1 mm/rev can cause wider residual stress gradients than at the lower feed of 0.05 mm/rev.

4.2.2.3 Quantitative analysis of residual stress gradients The calculated values for the residual stress gradients (for a new tool and a tool with a wear zone) and the measured values were analysed in terms of quantities such as the surface residual stress, σ_{surf}, and the maximum compressive residual stress, σ_{comp}, and its location, D_{comp}. From Fig. 12, it can be seen that σ_{surf} and σ_{comp} can be predicted to within about 150 MPa, which can occur among experimental rep-

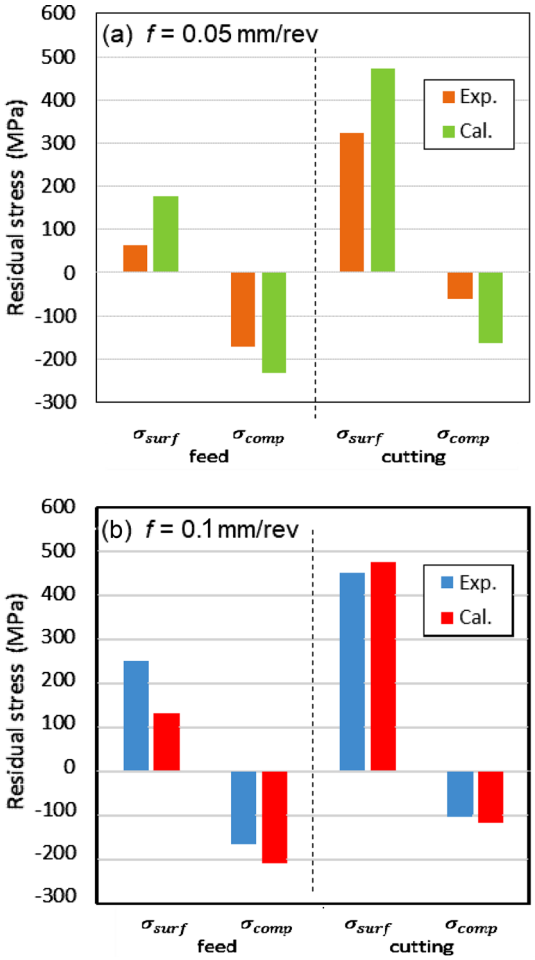

Fig. 12 Results of a quantitative analysis of the surface residual stress, σ_{surf}, and the maximum compressive residual stress, σ_{comp}: (**a**) $f = 0.05$ mm/rev, (**b**) $f = 0.1$ mm/rev

lications. The predictions for the higher feed rate seem to be more precise than for the lower rate. At the low feed of 0.05 mm/rev, this 3D model tends to overestimate the residual stress. In the 3D FEM zone with a low feed of 0.05 mm/rev in Fig. 8(a), the zone representing previous revolutions, marked "rev(r − 1)", has a smaller feed size. A study of the input parameters, such as mesh size refinement at lower feed of $f = 0.05$ mm/rev, may improve the predictions of σ_{surf} and σ_{comp}. The location of the maximum compressive residual stress, D_{comp}, could be predicted to within 10 µm.

4.2.3 Benchmarking to other residual stress data in residual stress modelings

Meurer et al. [13] studied the residual stress gradients using a 2D orthogonal cutting model of AISI4140 steel. Although it is hard to directly compare the residual stress data between 2D orthogonal cutting and 3D turning under different cutting conditions, it is valuable to benchmark the range of residual stresses found in the machining of AISI 4140 steel. In their study, they used cutting speeds of V_c = 50 and 100 m/min with uncut chip thicknesses of h = 0.05 and 0.1 mm. For orthogonal cutting with a cutting speed of V_c = 100 m/min, and $h = 0.05$ mm, the residual stress gradients (both experimental and calculated values) exhibited a tensile surface residual stress σ_{surf} of about 400 MPa and a maximum compressive residual stress σ_{comp} of about −300 MPa. These residual stresses are somewhat higher than those observed in Fig. 12, but the overall shapes in the study in [13] were similar to those found in this study.

The residual stress gradients in our study can also be compared to those reported for the turning of 15-5PH stainless steel in [8]. Although the machining conditions and materials for the two cases are different, the thermomechanical loadings and the corresponding residual stress quantities can be compared. In particular, the value of σ_{comp} (from three sets of measurements and calculations) in the feed direction ranged from about −400 to about −600 MPa. On the other hand, in this study, the calculated value of σ_{comp}, in the feed direction ranged from −208 to −233 MPa (Fig. 12). The difference in the values of the maximum normal stress, S22 (−1626 MPa in Fig. 8 vs. −3143 MPa in [8]) may explain this difference. Further comparative studies of different materials using this 3D hybrid model will contribute to a residual stress gradient database for industrial use.

4.2.4 Possible limitations of 3D hybrid residual stress modelling

The hybrid 3D residual model considered here employs a calibration procedure in which G_{FY} and G_{FZ} are applied to the thermomechanical loadings (Step 5 in Fig. 5). The values of G_{FY} and G_{FZ} can be found empirically by comparing experimentally measured and calculated residual stress gradients, as described in Sect. 4.2.2. It was found that the values of G_{FY} and G_{FZ} that yielded best fits to the experimentally measured residual stress gradients depended on the type of material and the machining parameters, such as the tool geometry and tool wear. For example, we can compare the G_{FY} and G_{FZ} values for the turning of 15-5PH stainless steel and AISI4140 steel as follows:

- For the machining (V_c = 120 m/min, $f = 0.2$ mm/rev) of 15-5PH stainless steel with a new tool [8], gain values of $G_{FY} = 1.40$ and $G_{FZ} = 1.68$ were used.
- For the machining (V_c = 200 m/min, $f = 0.05$ mm/rev) of AISI 4140 steel with a new tool in this study, gain values of $G_{FY} = 1.08$ and $G_{FZ} = 1.00$ were used.

When the calibration procedure for the reference cutting condition in this 3D hybrid residual stress model has been done, based on a simple turning test to measure the forces

(F_Y and F_Z) to obtain the gain values (G_{FY} and G_{FZ}), the use of the proposed model in industry to predict residual stress gradients in machining is straightforward and fast.

5 Conclusion

This study has presented a new 3D residual stress modelling procedure and has validated this model based on the turning of AISI 4140 steel with a newly developed software, MISULAB, using a 3D physical turned surface and 3D equivalent thermo-mechanical loadings. In general, when a new material is introduced at a particular site, the user needs to adopt values for the input parameters from the existing literature, or develop their own data from a residual stress calculation. However, developing a new constitutive law or a new friction model involves significant time and cost. The proposed 3D hybrid model can rapidly identify significant input parameters for residual stress calculations.

The following conclusions and transferable knowledge were obtained from this study:

- It was shown that the proposed hybrid 3D simulation model was capable of predicting residual stress profiles for the turning of AISI 4140 steel, a widely studied material.
- Experimental and simulated values for the residual stress gradients in AISI 4140 steel surfaces turned at low feed rates (f = 0.05 and 0.1 mm/rev) and small depth of cut (a_p = 0.2 mm) were reported.
- The effects of the feed rate on the residual stress gradients were explored.
- A consideration of the actual tool geometry, including a small wear zone of about 30 µm, was found to improve the prediction of the residual stress gradients at both feeds.

According to reviews [2, 22, 23] of the existing literature on the simulation of residual stresses in machining, there is a consensus that simulation based on chip formation involves a significant computational time and cost for industrial applications. This may pose an obstacle to the industrial use of existing models. The 3D hybrid residual stress model considered here can overcome these hurdles, and can be applied in industry. Moreover, Malakizadi et al. [22] recently stated that this 3D hybrid model approach could be used for the prediction of residual stresses with in situ sensor-based values (cutting force, F_Y, and penetration force, F_Z, which was measured by a dynamometer in this study).

Information such as tool geometry, material properties, thermo-mechanical loadings, experimental cuts and penetration forces can be saved in the server-based software MISULAB. This will allow users in industry to predict the residual stress gradients from their machining processes more easily and promptly.

The 3D hybrid model for predicting residual stress gradients can be adapted to consider other cases (processes, materials, tool wear/geometry, and coolant application), and this will form the subject of future work.

Supplementary Information The online version contains supplementary material available at https://doi.org/10.1007/s11740-023-01241-3.

Acknowledgements The authors are grateful to the MISU project for funding this research. Thanks are due to Vincent Lozano and Loïc Polly for their technical support regarding MISULAB. Special thanks to Karlsruhe Institute of Technology and professor, Volker Schulze for the provision of AISI 4140 bars and tool inserts for the CIRP surface conditioning project.

Declaration

Conflict of interest The authors declare that they have no conflict of interest.

References

1. Matsumoto Y, Hashimoto F, Lahoti G (1999) Surface integrity generated by precision hard turning. CIRP Annals, 48–1, pp 59–62
2. Elsheikh AH, Shanmugan S, Muthuramalingam T, Thakur AK, Essa FA, Ibrahim AMM, Mosleh AO (2022) A comprehensive review on residual stress in turning. Adv Manuf 10:287–312
3. Ee KC, Dillon OW Jr, Jawahir IS (2005) Finite element modelingof residual stresses in machining induced by cuttingusinga tool with finite edge radius. Int J Mech Sci 47:1611–1628
4. Nasr MNA, Ng EG, Elbestawi MA (2007) Modelling the effects of tool-edge radius on residual stresses when orthogonal cutting AISI 316L. Int J Mach Tools Manuf 47:401–411
5. Magalhaes FC, Ventura CEH, Abrao AM, Denkena B (2020) Experimental and numerical analysis of hard turning with multichamfered cutting edges. J Manuf Process 49:126–134
6. Valiorgue F, Rech J, Hamdi H, Gilles P, Bergheau JM (2012) 3D modeling of residual stresses induced in finish turning of an AISI304L stainless steel. Int J Mach Tools Manuf 53:77–90
7. Mondelin A, Valiorgue F, Rech J, Coret M 3D hybrid Numerical Model of residual stresses: Numerical—Sensitivity to cutting parameters when turning 15-5PH Stainless Steel. J Manufactruing Mater Process, 5–70;1–16, 2021.
8. Dumas M, Fabre D, Valiorgue F, Kermouche G, Van Robaeys A, Girinon M, Brosse A, Karaouni H, Rech J (2021) 3D numerical modelling of turning-induced residual stresses – A two-scale approach based on equivalent thermo-mechanical loadings. J Mater Process Technol 297:117274:1–13
9. Jawahir IS, Brinksmeiern E, M'Saoubi R, Aspinwall DK, Outeiro JC, Meyer D, Umbrello D, Jayal AD (2011) Surface integrity in material removal processes: recent advances. CIRP Ann 60(2):603–626
10. Ambrosy F, Zanger F, Schulze V (2015) FEM-simulation of machining induced nanocrystalline surface layers in steel surfaces prepared for tribological applications. CIRP Ann 64(1):69–72

11. González G, Segebade E, Zanger F, Schulze V (2019) FEM-based comparison of models to predict dynamic recrystallization during orthogonal cutting of AISI 4140. Procedia CIRP 82:154–159
12. Tekkaya B, Meurer M, Dölz M, Könemann M, Münstermann S, Bergs T (2023) Modeling of microstructural workpiece rim zone modifications during hard machining. J Mater Process Technol 311:117815
13. Meurer M, Tekkaya B, Schraknepper D, Bergs T, Münstermann S (2022) Numerical prediction of machining induced residual stresses when hard cutting AISI 4140. Procedia CIRP 108:583–588
14. Zielinski T, Vovk A, Riemer O, Karpuschewski B (2022) Influence of local material loads on surface topography while machining steel 42CrMo4 and inconel 718. Procedia CIRP 108:412–417
15. Rami A, Kallel A, Sghaier S, Youssef S, Hamdi H Residual stresses computation induced by turning of AISI 4140 steel using 3D simulation based on a mixed approach. Int J Adv Manuf Technol, 91:3833–38502017
16. Cedric C (2011) Vers une modélisation physique de la coupe des aciers spéciaux: intégration du comportement métallurgique et des phénomènes tribologiques et thermiques aux interfaces (in French). PhD thesis, Ecole Centrale de Lyon,
17. Aridhi A, Perrad T, Valiorgue F, Courbon C, Rech J, Brosse A, Girinon M, Truffart B, Karaouni H (2022) Comparison of the CEL and ALE approaches for the simulation of orthogonal cutting of 15-5PH and 42CrMo4 materials. Proc Institution Mech Eng Part B J Eng Manuf. https://doi.org/10.1177/09544054221136390. November
18. Capello E (2005) Residual stresses in turning: part I: influence of process parameters. J Mater Process Technol 160(2):221–228
19. Sharman AR (2006) An analysis of the residual stresses generated in Inconel 718™ when turning. J Mater Process Technol 173(3):359–367
20. Roy S, Kumar R, Das RK, Sahoo AK (2018) A comprehensive review on machinability aspects in hard turning of AISI 4340 steel. IOP Conference Series: Materials Science and Engineering, 390:012009,
21. Schulze V (2022) Surface conditioning in cutting and abrasive processes. The International Academy for Production Engineering
22. Malakizadi A, Bertolini R, Ducobu F, Kilic ZM, Magnanini MC, Shokrani A (2022) Recent advances in modelling and simulation of surface integrity in machining–a review. Procedia CIRP 115:232–240
23. Melkote S, Liang SY, Ozel T, Jawahir IS, Stephenson DA, Wang B (2022) A review of advances in modeling of conventional machining processes: from merchant to the present. J Manuf Sci Eng 144:110801–110801